1 *Article*

2 Chemical Vapour Deposition Graphene Field-Effect
3 Transistors for Detection of Human Chorionic
4 Gonadotropin Cancer Risk Biomarker

5 **Carrie Haslam[1], Samar Damiati[2], Toby Whitley[1], Paul Davey[1], Emmanuel Ifeachor[1] and Shakil A.**
6 **Awan[1,*]**

7 [1] Wolfson Nanomaterials and Devices Laboratory, School of Computing, Electronics and Mathematics,
8   Faculty of Science and Engineering, University of Plymouth, PL4 8AA, UK;
9 [2] Department of Biochemistry, Faculty of Science, King Abdulaziz University (KAU), Jeddah, Saudi Arabia;
10 * Correspondence: shakil.awan@plymouth.ac.uk; Tel.: +44(0)1752 586 325

11 **Abstract:** We report on the development of chemical vapour deposition (CVD) based graphene
12 field effect transistor (GFET) immunosensors for the sensitive detection of Human Chorionic
13 Gonadotropin (hCG), a glycoprotein risk biomarker of certain cancers. The GFET sensors were
14 fabricated on Si/SiO_2 substrate using photolithography with evaporated chromium and sputtered
15 gold contacts. GFET channels were functionalized with a linker molecule to immobile anti-hCG
16 antibody on the surface of graphene. Binding reaction of the antibody with varying concentration
17 levels of hCG antigen demonstrated the limit of detection of the GFET sensors to be below 1 pg/mL
18 using four-probe electrical measurements. We also show annealing can significantly improve the
19 carrier transport properties of GFETs and shift the Dirac point (Fermi level) with reduced p-doping
20 in back-gated measurements. The developed GFET biosensors are generic and could find
21 applications in a broad range of medical diagnostics in addition to cancer, such as
22 neurodegenerative (Alzheimer's, Parkinson's and Lewy body) and cardiovascular disorders.

23

24 **Keywords:** Graphene, Electrochemical Biosensors, Cancer, Diagnosis, Electrical Detection,
25 Alzheimer's Disease, Dementia, Neurodegenerative Disorders, Cardiovascular, Blood Biomarkers,
26 Antibodies, Proteins

27

28 1. Introduction

29   Since the discovery and isolation of graphene from graphite in 2004, the two-dimensional
30 material has shown potential to revolutionise many technological areas owing to its remarkable
31 electrical, optical, mechanical and thermal properties [1-3]. Graphene is a mono-atomic, planar
32 network of sp^2-bonded carbon atoms arranged in a honeycomb lattice. In particular, its chemical
33 stability, low electrical noise, significant surface-to-volume ratio, biocompatibility and field-effect
34 make graphene potentially an ideal platform for a variety of biosensing applications [4]. The
35 extraordinary surface-to-volume ratio of graphene facilitates a high density of disease specific
36 capture molecules or antibodies to be chemically immobilised onto its surface via covalent or
37 non-covalent functionalisation techniques. A key benefit of the latter is that the electrical transport
38 properties of graphene are not degraded as the mobility and carrier properties are maintained. This
39 can enhance the sensitivity of the biosensor and thereby improve its limit of detection (LoD).
40 Currently, a number of biosensor techniques are being explored to detect the presence of a given
41 biomarker, such as electrical, optical, resonant, acoustical, quartz crystal microbalance and surface
42 plasmon resonance (SPR) [5]. Whilst each technique has its advantages and disadvantages, the

43 electrical technique we are exploring offers some key benefits that make it a prime candidate for
44 eventual point-of-care (PoC) applications in the detection of specific cancer biomarkers and early
45 diagnosis. These include, label-free detection, high sensitivity, multiplexing, low-cost and
46 integration with a range of existing electronic systems. In contrast with our field-effect transistor
47 (FET) biosensors, there are also other electrical techniques, such as cyclic voltammetry (CV),
48 impedimetry and ampereometry functioning to detect a variation in resistance and/or capacitance,
49 that may be comparable to the FET approach in terms of sensitivity. The developed FETs will be
50 generic sensors and are therefore expected to have numerous other applications ranging from
51 neurodegenerative disorders (ND), such as Alzheimer's [6] and other dementias, and cardiovascular
52 to infectious diseases and environmental monitoring.

53   Here we report on the chemical vapour deposition (CVD) graphene field-effect transistor
54 (GFET) biosensors aimed at detecting the presence of Human Chorionic Gonadotropin (hCG)
55 protein biomarkers in samples from patients at different stages of disease progression. The
56 proof-of-concept GFETs were functionalized with monoclonal anti-hCG antibodies for the detection
57 of hCG protein biomarkers, label-free. hCG is a glycoprotein hormone (37-kDa) and its concentration
58 level serves as a clinical marker associated with testicular, pancreatic and prostate cancer [7-9], as
59 well as pregnancy. As with many diseases, early cancer recognition and diagnosis can be critical for
60 treatment and management to be effective, as well as enabling optimum health care provision and
61 potentially opening novel routes to be investigated to prevent the development of the disease
62 [10-12]. There is therefore an urgent need to develop diagnostic sensors and analytical tools for the
63 accurate identification and early diagnosis of cancer. hCG is composed of two subunits α and β,
64 which are non-covalently linked by hydrophobic and ionic interactions. The α subunit is known to
65 be common and the β subunit is unique to hCG, conferring biological activity to the hormone. The β
66 subunit is composed of 145 amino acids [13-17]. As a pregnancy biomarker hCG is usually secreted
67 by the trophoblast cells of the placenta peaking at ~ 10 weeks within the human gestation period.
68 The chief function of hCG is considered to maintain the corpus luteum and promote the production
69 of progesterone during pregnancy by the ovarian granulosa cells, whilst endorsing foetal growth
70 [18-22]. A typical, commercial biosensor that is designed to detect hCG and establish pregnancy
71 exhibits sensitively down to a nano-molar range [23]. It has been previously estimated that 95% of
72 pregnancies can be detected at a sensitivity of 1.24 µg/mL at the time of an expected menstrual
73 period [24-25]. Our GFET biosensors detailed here exhibit a significantly lower limit of detection of
74 ~0.1 pg/mL (determined using a 4-probe electrical technique) compared to a commercial biosensor
75 designed specifically for hCG detection. There are number of other studies that have investigated
76 antibody-antigen biomarker detection to analyse the necessary LoD of their sensors, e.g. Heideman
77 *et al.* [26], where they developed a Mach-Zehnder interferometer (MZI) immunosensor, based on a
78 silicon substrate with a detection limit of 50pM [26,27] and Mao et al., where they detected
79 immunoglobulin G (IgG) at the 2ng/mL level [28]. In respect to hCG detection via graphene, Teixeira
80 *et al.* [15] applied chemically-modified multi-layer epitaxial graphene to serve as the sense electrode
81 (functionalized with APTES). The device displayed a LoD of 0.62 ng/mL [15]. In addition, Teixeira *et*
82 *al* produced an immunosensor based on screen-printed electrodes (SPEs), with graphene functioning
83 as the working electrode to detect hCG. The LoD was determined to be 0.286 pg/mL [29]. In addition,
84 Islam et al. reported hCG detection limit of ~ 1 pg/mL using a CVD graphene biosensor [30]. The
85 developed GFET biosensors will also need to be validated against the gold standard in the field, that

86   of immunoassay enzyme-linked immunosorbent assay (ELISA) for both sensitivity and specificity.
87   In addition, since performing ELISA tests can be time consuming, requires high level of operator
88   expertise and complex equipment, making it expensive, we envisage that GFET biosensors could
89   present a potential low-cost, fast, accurate and reliable alternative technology platform.

90   **2. Materials and Methods**

91   Monolayer Graphene on a SiO_2/Si wafer was purchased from Graphenea (Spain). The required
92   chemicals applied for GFET fabrication were photoresist (PR), lift-off resist (LoR), Microposit
93   developer and Microposit remover, all purchased from A-Gas Electronic Materials (Warwickshire,
94   UK).

95   The hCG antigen and complementary anti-hCG monoclonal antibody were purchased from
96   Abcam *(UK).* The stocks were stored at −20 °C. Linker molecule 1-pyrenebutanoic acid succinimidyl
97   ester (Pyr-NHS) and bovine serum albumin (BSA) blocking solution were purchased from Sigma
98   Aldrich *(Dorset, UK).* Phosphate-Buffered Saline (PBS) tablets were purchased from Sigma Aldrich
99   *(Germany).*

100   Electrical characterisation and analysis were implemented under ambient conditions via a
101   Keysight B1500A semiconductor device parameter analyser, in conjunction with a Cascade
102   Microtech MPS150 probe station *(Thiendrof, Germany).* Current-voltage measurements (I_D-V_D and
103   I_D-V_G) were executed as a function of gate voltage (V_G) from - 100 V to + 100 V. The I_D-V_D curves were
104   acquired from - 100 mV to + 100 mV. The I_D-V_D and I_D-V_G curves were measured for each separate
105   functionalisation stage.

106   Graphene characterisation was performed using an XPLORA Raman spectroscopy system
107   *(HORIBA, UK).* The XPLORA system operated at a wavelength of 532 nm, with ~ 4 mW of incident
108   power. The XPLORA Raman system was combined with an OLYMPUS BX41 microscope *(Olympas,*
109   *Japan).*

110   To define and develop the necessary graphene channels and metallic contacts of Chromium
111   (Cr) and Gold (Au), the Mask aligner J500/VIS *(OAI optical associates Inc)* was deployed. A
112   conventional fan oven *(WTB binder, Germany)* was employed to perform necessary annealing
113   processes, as well as for pre- and post-baking stages during the photolithography processes. The
114   Hotplate SH8 *(STUART SCIENTIFIC)* and Ultrasonic Cleaner *(CBEST, US)* were used for pre- and
115   post-baking procedures and PR removal, respectively. An Argon (Ar) plasma etching technique
116   was used for graphene channel formation by means of a three target, 6-inch sputtering machine
117   *(Nordiko Limited, UK).* To aid in the formation of robust, metallic electrodes, an Edwards Thermal
118   Evaporator was deployed for the evaporation of Cr.

119   *2.1. Fabrication of CVD Graphene FETs*

120   The GFETs were fabricated using high quality CVD graphene to form transducer channels on
121   Si/SiO_2 substrate. A conventional photolithographic patterning and metal lift-off technique was used
122   to form the necessary graphene channels, as well as the source, drain and voltage sense electrodes.
123   The fabrication process involved spin-coating the CVD graphene samples with Lift-off Resist (LOR)
124   at 3000 revolutions-per-minute (RPM) for a few seconds. The samples were then placed in a fan oven
125   for pre-baking. The purpose of the pre-bake was to densify the LOR to assist with the formation of
126   clear, graphene channels. Subsequently, the samples were dried at ambient temperature. Next, the
127   samples were spin-coated with a layer of positive Photoresist (PR). Immediately after PR deposition,

128 the samples were post-baked on a hotplate. The hotplate solidifies the PR and removes any solvents
129 remaining on the samples. This process generated ~ 500 nm of PR film on the surface of graphene.
130 Successively, the coated samples were positioned in a mask aligner and exposed to ultra-violet (UV)
131 radiation for lithographic patterning of graphene channels. The UV exposed samples were also
132 submerged in a chemical developer before being placed in a vacuum chamber to dry. Alternatively,
133 the samples can be left to dry at ambient temperature, outside of the vacuum chamber. An
134 additional post-baking stage was applied to the samples following the drying and placed on a
135 hotplate under an intermittent deep ultraviolet source (DUV). This exposure to DUV can reduce the
136 quantity of PR/PMMA residue on the substrate surface prior to plasma etching, whilst reducing
137 contact resistance.

138 The chemically developed and dried samples were transferred into a sputtering machine and
139 exposed to Ar plasma etching for few minutes. Throughout the process, the inert Ar gas functions
140 as the gaseous etchant and removes the exposed regions of graphene, whilst leaving behind the
141 shaped graphene channels (previously coated and protected with PR). Graphene shaping is
142 effectively complete after an etching time of a few minutes at high power. The sputtering machine
143 was also used to sputter and form the associated metallic electrodes, 30 nm of Au. Following
144 successful shaping, the samples were transferred to a chemical remover to dissolve the LoR and PR
145 remaining on the substrate to expose the graphene channels. The samples were immersed in the
146 chemical remover, whilst located in an ultrasonic bath for ~2 hour at ~60°C. The samples were
147 subsequently rinsed and bathed in de-ionised water and transferred into a vacuum chamber to dry
148 for few hours.

149 For the final stage of GFET fabrication, metallic Cr and Au electrodes were formed on the
150 graphene channels. The samples were post-baked in a fan oven, instead of being irradiated with
151 DUV. This post-baking stage is necessary to remove the solvents located within the PR and
152 eliminate any additional water. Following photolithography, thermal evaporation of Cr was
153 performed using an Edwards Thermal Evaporator for a few seconds. The Cr functions as an
154 adhesive layer between graphene and the Au metallic contacts. The Cr target material was heated
155 to ~2000°C and evaporated within a high vacuum. The heated coil of Cr is applied to form a thin
156 film of ~5 nm on the surface of the graphene samples. The metallic contacts are fully formed after
157 sputtering 30 nm of Au on the Cr film. After the Au sputtering process, the initial chemical remover
158 step is repeated and the final samples are dried in a vacuum chamber for a few hours, prior to
159 electrical characterisation.

160 For this study a number of CVD graphene samples were fabricated. Each sample consisted of
161 fifteen GFET devices (with an area of ~1 cm^2) in total, i.e. five GFET devices consisted of five
162 asymmetric Cr/Au voltage sense electrodes with an associated graphene channel length of 720 μm,
163 whereas the remaining ten GFET devices consisted of six symmetric voltage sense electrodes with a
164 channel length of 300 μm, as shown in Fig. 1. The width of all GFET channels was fixed at 80 μm.

165

166

167

168

169

170

171

172

173

174

175
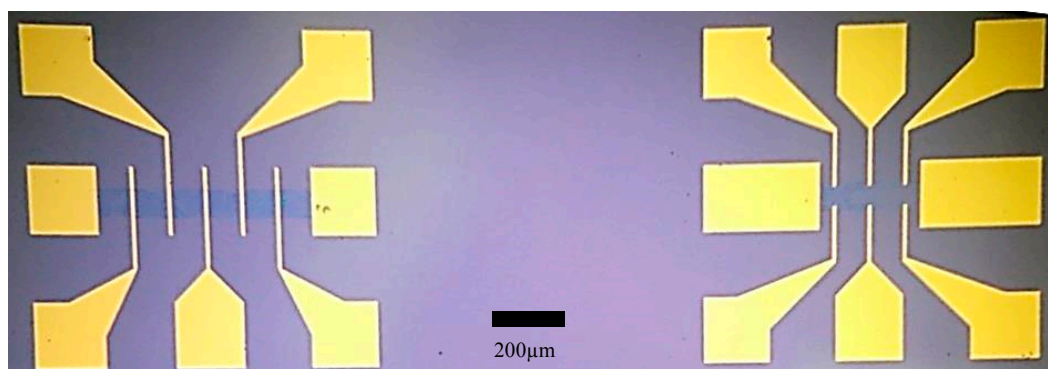
176   **Figure 1:** Graphene FET devices with asymmetric (left) and symmetric (right) voltage sense

177   electrodes. Graphene channels, in the central regions of the FET devices, have a dark blue contrast

178   compared to the Si/SiO$_2$ substrate.

179   **3. Results**

180   *3.1. Characterisation of CVD Graphene using Raman Spectroscopy*

181   Raman spectroscopy was performed on two representative CVD samples to analyse the quality
182   of graphene and to estimate various properties, such as number of layers [31], doping and residues
183   from the fabrication process. Random spot Raman measurements were carried out at the central
184   region of bare samples. The Raman spectra were measured with a 10X objective, under ambient
185   conditions with an incident power of ~ 4 mW and a wavelength of 532 nm. Figure 2 shows Raman
186   spectra from the two samples with an intensity ratio of the 2D peak to G peak of I(2D)/I(G) ~ 2 and
187   one sample shows a significant D peak, whereas it is absent in the other. The intensity ratio
188   I(2D)/I(G), position and full width half maximum (FWHM) of the G and 2D peaks confirm presence
189   of monolayer graphene. The presence and intensity of the D peak in one of the samples also indicates
190   that the graphene in that sample contains defects. Raman mapping of a few regions of the graphene
191   wafer (before it was diced into 1cm^2 samples) confirmed majority of the regions consisted of
192   mono-layer graphene.

193   *3.2. Electrical Characterisation of GFETs*

194   The GFETs were characterized using 2-probe, 4-probe and back-gated measurements under ambient
195   conditions. The bare GFETs (i.e. without any biomolecule functionalization) were first measured to
196   extract the I$_D$-V$_D$ characteristics of the fifteen devices on each 1 cm^2 sample. A comparison between
197   2-probe, 4-probe and back-gated data enabled us to extract the contact resistance, mobility and
198   sheet resistance of the graphene channels within the GFET devices. A typical 4-probe I$_D$-V$_D$ and
199   I$_D$-V$_G$ measurements from a GFET sensor using a Keysight parameter analyser interfaced to a
200   Cascade probe station is shown in Fig. 3. The I$_D$-V$_D$ data shows approximate linear response over
201   the ± 60 mV range and a slight non-linearity beyond this range probably due to Schottky contacts or
202   charge traps at the interface with the Si/SiO$_2$ substrate [32]. This is further confirmed from the I$_D$-V$_G$
203   data which shows a characteristic hysteretic behavior due to the presence of charge traps at the
204   interface. The Dirac point is found to vary from 50 V to 80 V depending on the voltage sweep and
205   its positive magnitude indicates the graphene channel is p-doped (at V$_D$ = 100 mV). The 4-probe
206   resistance of the graphene channel is found to be ~700 Ω (with gate potential at 0V), whereas the
207   mobility is approximately 1200 cm^2/Vs.
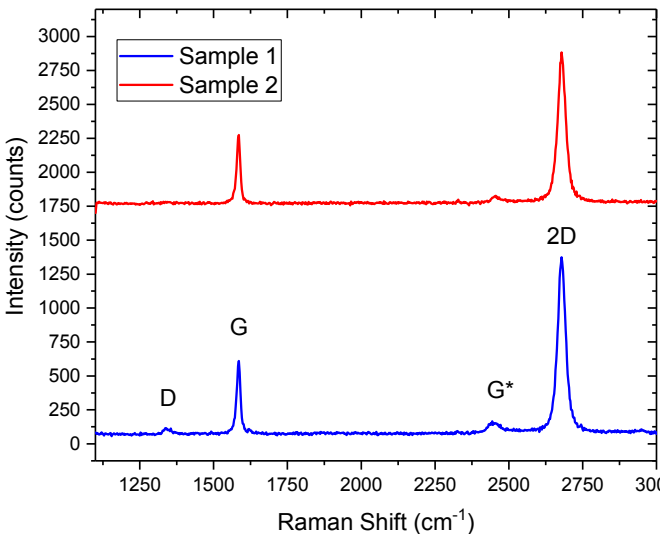
Figure 2: Raman Spectra of quality and defected CVD graphene before being deployed as the transducer element in a GFET biosensor. The defected sample (blue) shows a prominent D-band.

We have also explored the effect of annealing on our devices in order to improve the overall performance of the bare GFET sensors. Figure 4 displays the results from one device before and after annealing. Before annealing the device showed relatively low conduction level and its Dirac point was in excess of 40 V. However, after annealing the sample, the Dirac point could now be discerned and shifted to approximately 23 V (with p-type doping). This is likely due to desorption of oxygen and water molecules from the surface of graphene [33-35]. In pristine graphene, the Dirac point would ideally be located at zero gate voltage. A Dirac point situated relatively far from the zero point indicates unintentional doping, which could be due to the fabrication process. The location of the Dirac point is dependent on the difference between the work function of the gate, metallic contacts, and the graphene channel, as well as doping and the presence of biomolecules adsorbed on the surface [36]. From the knowledge of the Dirac point and shape of the I_D-V_G curve near its vicinity, a number of properties of the channel can be estimated, such as mobility, doping, defects etc.
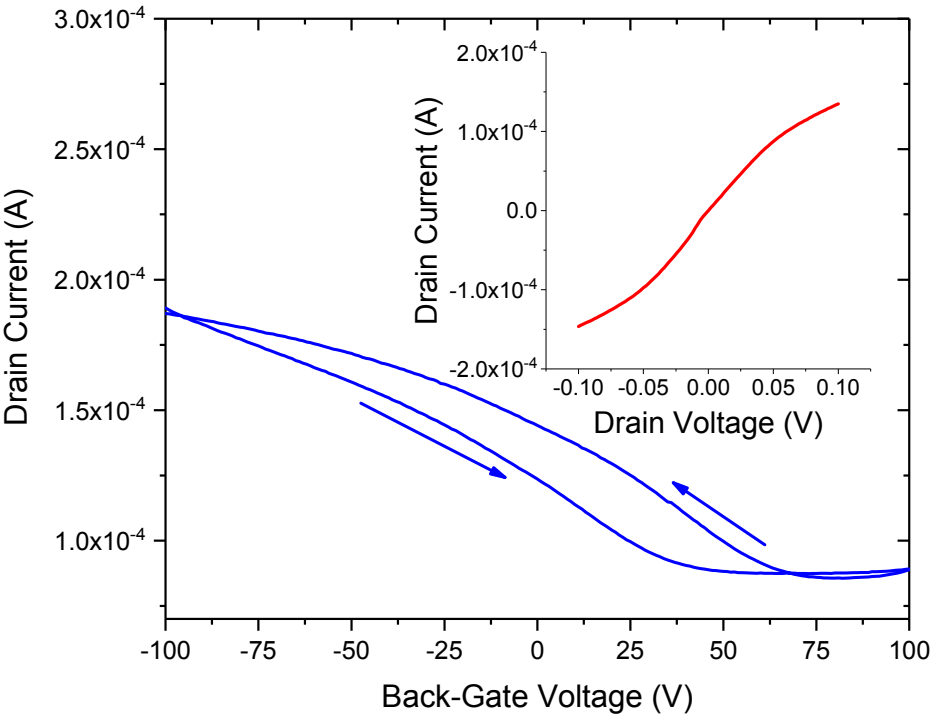
266   **Figure 3**: I_D-V_G at V_D = 100 mV and the corresponding I_D-V_D (inset) of a CVD graphene FET sensor.
267   The arrows indicate forward and reverse sweep of the back-gate voltage showing hysteretic
268   behavior.
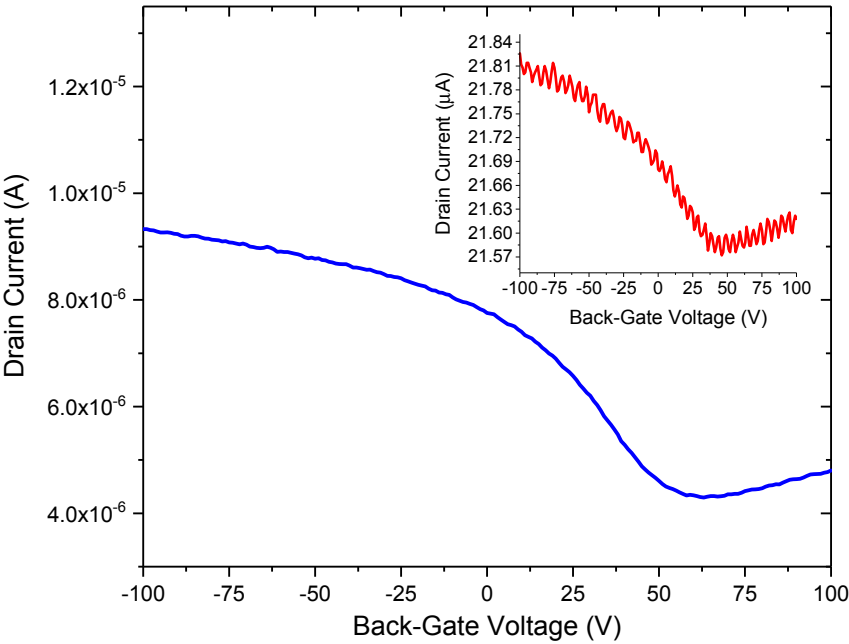
281   **Figure 4**: Annealed I_D-V_G curve of a CVD graphene FET and its corresponding
282   I_D-V_G (inset) before annealing, both at V_D = 100 mV.

3.3. Functionalisation of GFETs

To facilitate antibody (Ab) immobilization, we used a linker molecule Pyr-NHS ester. The linker retains a succinimidyl ester group, which interacts with the amino groups on the anti-hCG Ab surface to generate a stable, amide bond. In addition, the Pyr-NHS has an aromatic pyrenyl group, which can strongly interact with the graphene surface, via a non-covalent π-π stacking. Non-covalent binding is dependent on physical adsorption of the biomolecule, using hydrophobic, hydrophilic, electrostatic and van der Waals interactions. Thus, Pyr-NHS ester causes the pyrene group at one end of the linker to strongly bind to the graphene surface via π-π interactions and the succinimidyl ester group will covalently react with the amino group (NH_2) of the Ab without requiring a high pH [37]. The non-covalent attachment of Pyr-NHS ester with graphene does not disrupt the electrical properties of graphene, whereas covalent bonding can lead to scattering and the introduction of impurities in the graphene sp^2 lattice. This type of immobilisation typically leads to a self-assembled monolayer (SAM) of molecules on the surface of graphene, although the Abs may remain randomly orientated.

The GFET devices were biologically modified and converted into biosensors via the drop casting of biomolecules. Initially, Pyr-NHS ester linker molecules were applied to cover the surface of the graphene channels at a concentration of 2 mM. The samples were incubated at low temperature for a few hours before rinsing with PBS and drying at ambient temperature. Once the samples were dry, electrical characterisation was performed. Following attachment of Pyr-NHS ester and electrical characterisation, anti-hCG Ab was applied to the samples and again incubated before rinsing with PBS and drying at ambient temperature. The same process was repeated for BSA deposition. BSA was applied to block additional sites between the Ab regions which prevents
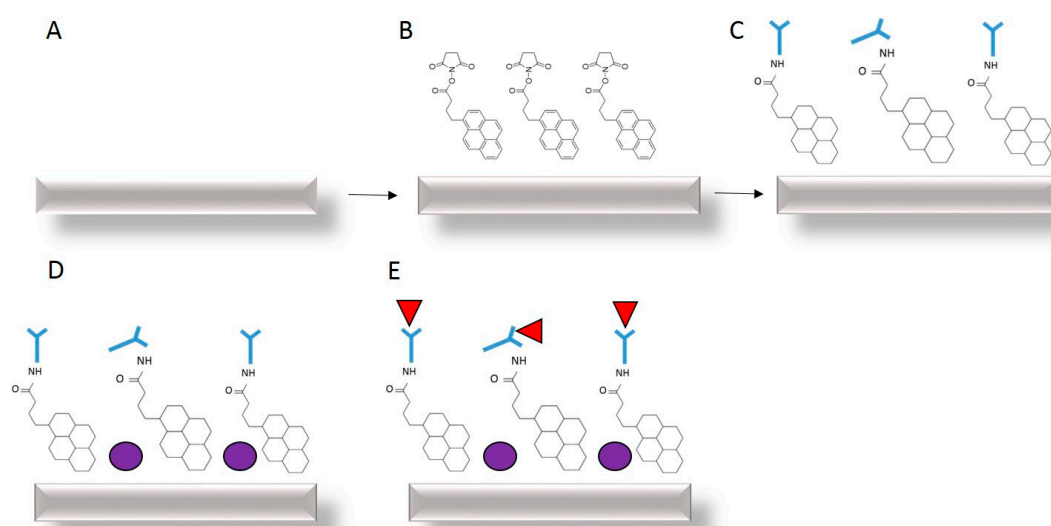
Figure 5: GFET functionalisation and measurement of (A) bare graphene (B) non-covalent attachment of Pyr-NHS ester linkers with graphene (C) anti-hCG antibody (light blue) attachment to the linkers (D) BSA blocking (dark blue) and (E) detection of hCG antigen (red) binding with the antibody. Each stage is characterised using 4-probe electrical measurements of I_D-V_D and I_D-V_G.

314   non-specific binding. Finally, hCG antigen was applied to the samples at a concentration ranging
315   from 0.1 pg/mL to 1 ng/mL and characterised using 4-probe electrical measurements. Samples were
316   then incubated at ambient conditions for 1 hour, prior to a PBS rinse. Figure 5 illustrates the steps
317   involved within the functionalisation process.

318   *3.4. Atomic Force Microscopy of Functionalised GFETs*

319   Further characterisation of the functionalised GFETs was performed using Atomic Force
320   Microscopy (AFM, *Pacific Nanotechnology* and probe tips from *Nano World*). Multiple AFM images
321   were generated in respect to the various necessary functionalisation steps. The difference in height
322   and morphology at hCG functionalisation stage is displayed in Figure 6. The AFM image illustrates
323   the successful immobilisation of Pyr-NHS linker, Ab, BSA and the corresponding hCG antigen
324   molecules on the surface of the graphene FETs. The hCG antigen is measured to be ~7-10 nm in
325   height.

326
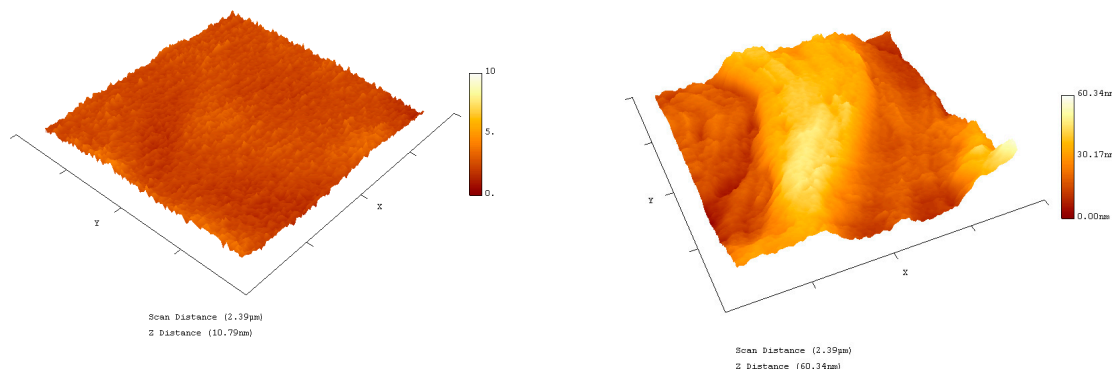
333   **Figure 6**: AFM image of bare graphene on Si/SiO2 (left) and functionalised with Pyr-NHS
334   linker, Ab, BSA and the corresponding hCG antigen (right).

335

336   *3.5. Scanning Electron Microscopy of Functionalised GFETs*

337   SEM Image (using a JOEL JSM-7001F) shows a GFET device with 10 pg/mL of hCG antigen on the
338   surface of graphene, including immobilisation of Pyr-NHS ester linker and functionalised with Ab
339   and BSA blocking molecules. The image (taken at 25,000 times magnification) shows hCG
340   appearance to be foam like with relatively large voids over the 5μm × 5μm region. The hCG
341   appears also not to be uniformly distributed, indicating further optimisation may be needed to
342   achieve a uniform distribution of the antigen on the surface of graphene to enable consistent and
343   repeatable response of the GFET biosensors.
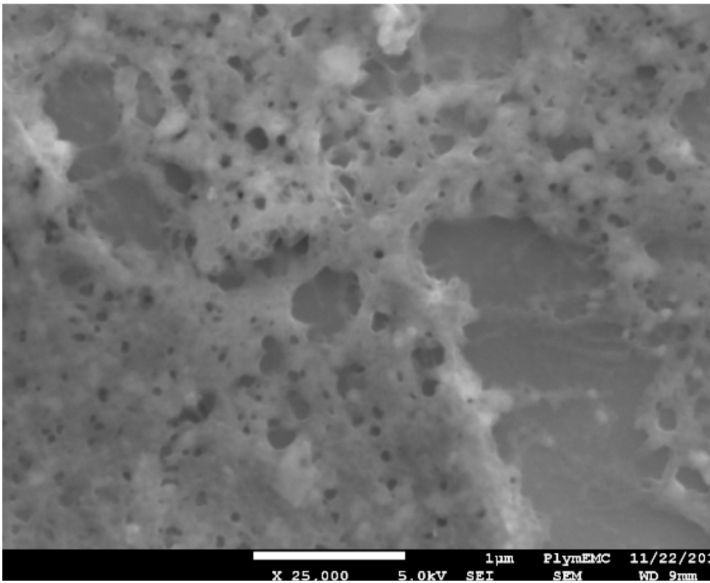
370   **Figure 7**: SEM image displaying bare graphene functionalised with Pyr-NHS linker, Ab, BSA
371   and the corresponding hCG antigen. Scale bar is 1 μm.
372

373   *3.6. Detection of hCG concentration*

374   The fabricated GFET sensors were characterised using 4-probe electrical measurements at each
375   stage of the functionalisation and binding interactions of the anti-hCG antibody with hCG antigen at
376   varying concentration levels of the latter. All measurements were performed in ambient conditions.
377   Figure 8 shows the response curves of two GFET biosensors when exposed to 1 pg/mL and 1 ng/mL
378   hCG antigen. The corresponding changes in resistance at each stage and concentration levels are
379   shown in Table 1. A striking feature of the results shown in Figure 8 and Table 1 is that whilst the
380   change in resistance coefficient ΔR for 1 pg/mL is positive for all stages of the functionalisation, this
381   is not the case for the 1 ng/mL concentration level. In this case, the coefficient is negative until
382   antibody binding stage but then becomes positive. This may be related to the complex interplay
383   between the potential distribution in the graphene channel, attached molecules and the interface
384   with the substrate. In addition, despite 3 orders-of-magnitude difference between the 1 pg/mL and
385   1 ng/mL concentration levels the change in resistance coefficient is ~114.1% and ~305%, respectively.
386   In contrast, we measured ΔR~135.9% for 10 pg/mL, ΔR~180.4% for 100 pg/mL and a LoD of the
387   sensors to be ~0.1 pg/mL, as shown in Fig. 9. The response of the GFET sensors to hCG antigen
388   concentration is found to be logorithmic (linear fit on a semi-log plot) over the 1 pg/mL to 1 ng/mL
389   range, as shown in Fig. 9. The least-square linear fit to the measured GFET 4-probe resistance change
390   shows reasonably good fit with R^2 ~0.8. The corresponding sensitivity of the GFET biosensors is
391   found to be ~(61.8±16.7)% / decade of hCG concentration over the 1 pg/mL to 1 ng/mL range. This
392   represents a significant sensitivity level for hCG antigen detection. However, it is worth highlighting
393   that our GFET biosensors have not yet been optimised for numerous parameters (mobility etc.) to
394   achieve even higher sensitivity levels and lower detection limits. These aspects are currently being
395   explored and will be reported on in subsequent future publications.
396   The data in Table 1 for the measured 4-probe resistance of the GFET sensors at 1 pg/mL and
397   1 ng/mL concentration levels also includes the change in resistance coefficient ΔR. This is calculated
398   relative to the two nearest stages, i.e. bare graphene to linker, linker to Ab, etc. The physical
399   mechanism for this change in resistance of the graphene channel at each functionalisation stage is
400   due to the attached molecules either donating or accepting electrons to/from the channel. Thus,

401   sensitivity of the sensors can be estimated from ΔR for hCG (or change in resistance from BSA to the
402   hCG analyte).

403

404

405

406

407

408

409

410
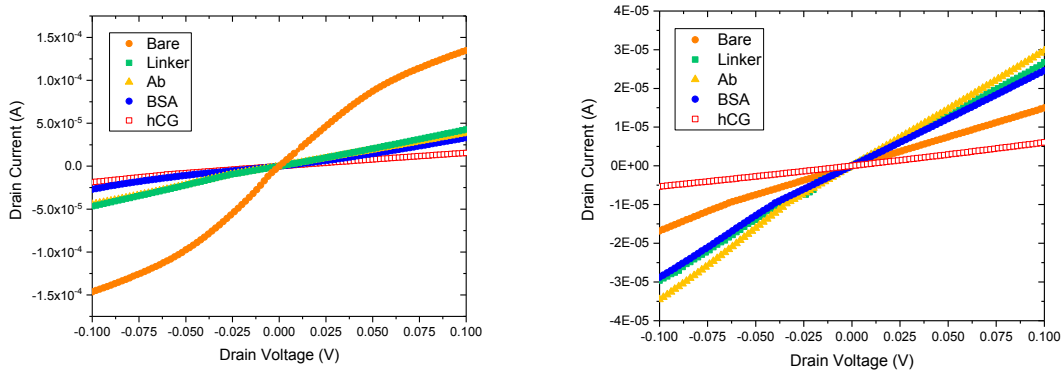
411   **Figure 8**: Characteristic I_D-V_D curves from the GFET sensors at different stages of biomolecule
412   exposure for 1pg/mL (left) and 1ng/mL (right) hCG concentration levels.

413
414
415   **Table 1.** Summary of GFET resistance changes measured at different stages of the
416   functionalisation process with 1pg/mL to 1ng/mL concentration of hCG antigen.

Stage	1pg/mL(Ω)	ΔR(%)	1ng/mL(Ω)	ΔR(%)
Bare	741.8	0	6686.3	0
Linker	2341.9	+215.7	3733.3	-44.2
Ab	2590.7	+10.6	3361.7	-11.1
BSA	3021.0	+16.6	4065.4	+20.9
hCG	6467.5	+114.1	16468.5	+305.1
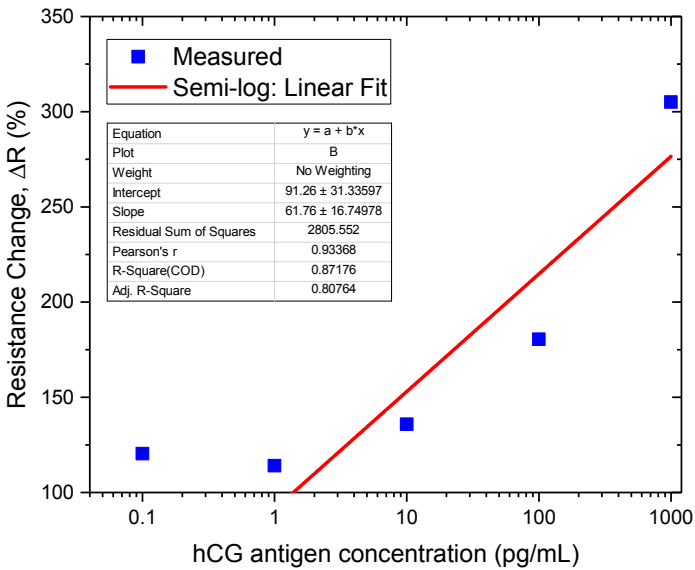
Figure 9: Measured resistance change coefficient with hCG concentration and a least-squares
linear fit (on a semi-log plot) to the data from 1 pg/mL to 1 ng/mL range.

4. Discussion

The CVD graphene FET biosensors have been characterised at all stages of the fabrication
process (Raman, AFM, electrical) and functionalisation (Raman, AFM, SEM, electrical) to establish a
robust and reproducible process for the development of the proof-of-concept sensors. Our data
presented in this study has demonstrated that CVD graphene FETs can sensitively detect hCG
antigen with approximately three to four orders of magnitude lower concentration level compared
to commercially available sensors. In addition, the GFET sensors can be operated in a resistive or
back-gated mode and in the future we aim to compare the sensitivity of these two approaches.
However, the data in Figure 8 shows clear characteristic curves for a resistive GFET sensor which we
also observed for the 10 and 100 pg/mL concentration levels of the hCG antigen. As shown in Figure
3, back-gated GFET sensor properties can be influenced due to the presence of water molecules on
the surface of graphene, charge traps at the interface between graphene and the supporting substrate
(in our case Si/SiO_2) leading to hysteretic effects. Therefore, a robust comparison of the resistive with
back-gated GFET sensors will require careful device design and optimisation.

Annealing of the GFET biosensors showed remarkable improvements in their electrical
performance, in terms of enhanced carrier transport properties and Dirac point shift due to oxygen
and water molecules being desorbed from the surface of graphene. Work is currently underway to
compare annealed devices with those that have been fabricated in the same batch but not annealed.
In addition, all the results reported in this study are based on direct current (DC) 4-probe resistance
measurements. We therefore anticipate further improvements in S/N can also be achieved using
alternating current (AC) or radio-frequency (RF) detection techniques [38,39].

5. Conclusions

We have demonstrated the use of CVD graphene FETs on Si/SiO$_2$ substrate as sensitive immunosensors for the proof-of-concept detection of hCG antigen, with a LoD below ~1 pg/mL. Although characteristic current-voltage response curves of the GFETs have been established, the sign of the resistance change coefficient ΔR has a strong dependence on the potential environment of the graphene channels. In addition, we have also shown that annealing the GFET sensors can significantly improve their performance and potentially lead to even more sensitive devices. In the near future the GFET biosensors will be explored for the detection of hCG biomarkers in case vs control samples from patients. Furthermore, in the next stage of development of the GFETs we will also investigate specificity of the sensors, optimisation of the quality of CVD graphene, contact resistance and novel AC and RF detection techniques to enhance the sensitivity of the biosensors.

Acknowledgements

We acknowledge funding from the UK's Engineering and Physical Sciences Research Council (EPSRC) under contract number EP/M006301/1 and the University of Plymouth, GD105227. SD would like to thank University of Plymouth, UK, for a guest-researcher position in summer 2017.

References

1. Novoselov, K.S., et al., *Electric field effect in atomically thin carbon films.* Science, 2004. **306**(5696): p. 666-9.
2. Geim, A.K., *Graphene: status and prospects.* Science, 2009. **324**(5934): p. 1530-4.
3. Geim, A.K. and P. Kim, *Carbon wonderland.* Sci Am, 2008. **298**(4): p. 90-7.
4. Forsyth, R., A. Devadoss, and O.J. Guy, *Graphene Field Effect Transistors for Biomedical Applications: Current Status and Future Prospects.* Diagnostics (Basel), 2017. **7**(3).
5. Allsop, T., et al., *Real-time kinetic binding studies at attomolar concentrations in solution phase using a single-stage opto-biosensing platform based upon infrared surface plasmons.* Opt Express, 2017. **25**(1): p. 39-58.
6. World Alzheimer's Report 2016. Publisher, *Alzheimer's Disease International*, September 2016.
7. Sánchez, S., et al., *Toward a fast, easy, and versatile immobilization of biomolecules into carbon nanotube/polysulfone-based biosensors for the detection of hCG hormone.* Analytical chemistry, 2008. **80**(17): p. 6508-6514.
8. Sinosich, M.J., H. Torode, and D. Saunders, *Diagnosis and management of extrauterine pregnancies.* Australian and New Zealand journal of obstetrics and gynaecology, 1993. **33**(3): p. 307-311.
9. Santandreu, M., S. Alegret, and E. Fabregas, *Determination of β-HCG using amperometric immunosensors based on a conducting immunocomposite.* Analytica Chimica Acta, 1999. **396**(2): p. 181-188.
10. Yang, W., et al., *Carbon nanomaterials in biosensors: should you use nanotubes or graphene?* Angewandte Chemie International Edition, 2010. **49**(12): p. 2114-2138.
11. Chen, A. and S. Chatterjee, *Nanomaterials based electrochemical sensors for biomedical applications.* Chemical Society Reviews, 2013. **42**(12): p. 5425-5438.

498 12. Pumera, M., *Graphene in biosensing.* Materials today, 2011. **14**(7): p. 308-315.

499 13. Pierce, J.G. and T.F. Parsons, *Glycoprotein hormones: structure and function.* Annual review of
500   biochemistry, 1981. **50**(1): p. 465-495.

501 14. Stenman, U.-H., et al., *The classification, functions and clinical use of different isoforms of HCG.*
502   Human reproduction update, 2006. **12**(6): p. 769-784.

503 15. Teixeira, S., et al., *Epitaxial graphene immunosensor for human chorionic gonadotropin.* Sensors
504   and Actuators B: Chemical, 2014. **190**: p. 723-729.

505 16. Netto, G.J. and J.I. Epstein, *Chapter 16 - Immunohistology of the Prostate, Bladder, Kidney, and*
506   *Testis A2 - Dabbs, David J*, in *Diagnostic Immunohistochemistry (THIRD EDITION).* 2011, W.B.
507   Saunders: Philadelphia. p. 593-661.

508 17. Cole, L.A., *Biological functions of hCG and hCG-related molecules.* Reproductive Biology and
509   Endocrinology : RB&E, 2010. **8**: p. 102-102.

510 18. Bahadır, E.B. and M.K. Sezgintürk, *Applications of electrochemical immunosensors for early*
511   *clinical diagnostics.* Talanta, 2015. **132**: p. 162-174.

512 19. Tsampalas, M., et al., *Human chorionic gonadotropin: A hormone with immunological and*
513   *angiogenic properties.* Journal of Reproductive Immunology, 2010. **85**(1): p. 93-98.

514 20. Cole, L.A., *hCG, five independent molecules.* Clinica chimica acta, 2012. **413**(1): p. 48-65.

515 21. Korevaar, T.I.M., et al., *Reference ranges and determinants of total hCG levels during pregnancy:*
516   *the Generation R Study.* European Journal of Epidemiology, 2015. **30**(9): p. 1057-1066.

517 22. Larsen, J., et al., *Human chorionic gonadotropin as a measure of pregnancy duration.* International
518   Journal of Gynecology & Obstetrics, 2013. **123**(3): p. 189-195.

519 23. Bahadır, E.B. and M.K. Sezgintürk, *Applications of commercial biosensors in clinical, food,*
520   *environmental, and biothreat/biowarfare analyses.* Analytical Biochemistry, 2015.
521   **478**(Supplement C): p. 107-120.

522 24. Cole, L.A., et al., *Accuracy of home pregnancy tests at the time of missed menses.* American journal
523   of obstetrics and gynecology, 2004. **190**(1): p. 100-105.

524 25. Gnoth, C. and S. Johnson, *Strips of Hope: Accuracy of Home Pregnancy Tests and New*
525   *Developments.* Geburtshilfe und Frauenheilkunde, 2014. **74**(7): p. 661-669.

526 26. Heideman, R., R. Kooyman, and J. Greve, *Performance of a highly sensitive optical waveguide*
527   *Mach-Zehnder interferometer immunosensor.* Sensors and Actuators B: Chemical, 1993. **10**(3): p.
528   209-217.

529 27. Fan, X., et al., *Sensitive optical biosensors for unlabeled targets: A review.* Analytica Chimica Acta,
530   2008. **620**(1): p. 8-26.

531 28. Mao, S.; et al., *Direct Growth of Vertically-oriented Graphene for Field-Effect Transistor Biosensor.*
532   Sci. Rep. 2013, **3**, 1696.

533 29. Teixeira, S., et al., *Label-free human chorionic gonadotropin detection at picogram levels using*
534   *oriented antibodies bound to graphene screen-printed electrodes.* Journal of Materials Chemistry B,
535   2014. **2**(13): p. 1852-1865.

536 30. Islam, K., A. et al., *A Label-Free and Ultrasensitive Immunosensor for Detection of Human*
537   *Chorionic Gonadotrophin Based on Graphene FETs.* Biosensors, 2017. **7**(3):27.

538 31. Ferrari, A.C., et al., *Raman spectrum of graphene and graphene layers.* Physical review letters,
539   2006. **97**(18): p. 187401.

540   32.   Di Bartolomeo, A., et al., *Graphene field effect transistors with niobium contacts and asymmetric*
541   *transfer characteristics.* Nanotechnology, 2015. **26**(47): p. 475202.
542   33.   Tien, D.H., et al., *Characterization of Graphene-based FET Fabricated using a Shadow Mask.*
543   Scientific reports, 2016. **6**: p. 25050.
544   34.   Chen, S., et al., *Adsorption/desorption and electrically controlled flipping of ammonia molecules on*
545   *graphene.* New Journal of Physics, 2010. **12**(12): p. 125011.
546   35.   Joshi, P., et al., *Intrinsic doping and gate hysteresis in graphene field effect devices fabricated on SiO2*
547   *substrates.* Journal of Physics: Condensed Matter, 2010. **22**(33): p. 334214.
548   36.   Chen, F., J. Xia, and N. Tao, *Ionic screening of charged-impurity scattering in graphene.* Nano
549   Letters, 2009. **9**(4): p. 1621-1625.
550   37.   Huang, Y., et al., *Graphene-based biosensors for detection of bacteria and their metabolic activities.*
551   Journal of Materials Chemistry, 2011. **21**(33): p. 12358-12362.
552   38.   Awan, S. A., et al., *Transport conductivity of graphene at RF and microwave frequencies.* 2D
553   Materials, 2016. **3**(1): p. 015010.
554   39.   Awan, S. A., et al., *Coaxial electrical circuits for interference-free measurements.* 2011, IET, ISBN:
555   978-1-84919-069-5.
556